Monthly Notices of the ROYAL ASTRONOMICAL SOCIETY

MNRAS **544,** L113–L120 (2025) https://doi.org/10.1093/mnrasl/slaf109
Advance Access publication 2025 October 27

Tentative rotation in a galaxy at $z \sim 14$ with ALMA

J. Scholtz [1,2★†], E. Parlanti,[3,4★†] S. Carniani [3], M. Kohandel [3], F. Sun,[5] A. L. Danhaive,[1,2] R. Maiolino [1,2,6], S. Arribas,[7] R. Bhatawdekar [8], A. J. Bunker,[9] S. Charlot [10], F. D'Eugenio [1,2], A. Ferrara,[3] Z. Ji,[11] Gareth C. Jones [1,2], P. Rinaldi,[11] B. Robertson,[12] A. Pallottini [3,13], I. Shivaei,[7] Y. Sun [11], S. Tacchella [1,2], H. Übler [4] and G. Venturi [3]

[1]*Kavli Institute for Cosmology, University of Cambridge, Madingley Road, Cambridge CB3 0HA, UK*
[2]*Cavendish Laboratory, University of Cambridge, 19 JJ Thomson Avenue, Cambridge CB3 0HE, UK*
[3]*Scuola Normale Superiore, Piazza dei Cavalieri 7, I-56126 Pisa, Italy*
[4]*Max-Planck-Institut für Extraterrestrische Physik (MPE), Gießenbachstraße 1, D-85748 Garching, Germany*
[5]*Center for Astrophysics | Harvard & Smithsonian, 60 Garden Street, Cambridge, MA 02138, USA*
[6]*Department of Physics and Astronomy, University College London, Gower Street, London WC1E 6BT, UK*
[7]*Centro de Astrobiología (CAB), CSIC-INTA, Cra. de Ajalvir Km. 4, E-28850 Torrejón de Ardoz, Madrid, Spain*
[8]*European Space Astronomy Centre (ESAC), European Space Agency (ESA), Camino Bajo del Castillo s/n, E-28692 Villanueva de la Cañada, Madrid, Spain*
[9]*Department of Physics, University of Oxford, Denys Wilkinson Building, Keble Road, Oxford OX1 3RH, UK*
[10]*Sorbonne Université, CNRS, UMR 7095, Institut d'Astrophysique de Paris, 98 bis bd Arago, F-75014 Paris, France*
[11]*Steward Observatory, University of Arizona, 933 N Cherry Avenue, Tucson, AZ 85721, USA*
[12]*Department of Astronomy and Astrophysics, University of California, Santa Cruz, 1156 High Street, Santa Cruz, CA 96054, USA*
[13]*Dipartimento di Fisica 'Enrico Fermi', Universitá di Pisa, Largo Bruno Pontecorvo 3, I-56127 Pisa, Italy*

Accepted 2025 October 17. Received 2025 September 22; in original form 2025 February 21

ABSTRACT

We reanalysed the Atacama Large Millimeter/submillimeter Array (ALMA) observations of the [O III] λ88 μm emission line in JADES-GS-z14-0, so one of the most distant spectroscopically confirmed galaxies at $z = 14.18$. Our analysis shows a tentative detection of a velocity gradient of [O III] λ88 μm using three independent tests: (1) construction of moment maps; (2) extraction of integrated spectra from a grid of apertures; and (3) spectro-astrometry in both the image and *uv* planes, confirming the presence of the velocity gradient at 3σ significance. We performed kinematical fitting using the KINMS code and estimated a dynamical mass of $\log_{10}(M_{\rm dyn}/{\rm M}_\odot) = 9.4^{+0.8}_{-0.4}$, with the bulk of the uncertainties due to the degeneracy between dynamical mass and inclination. We measure an upper limit on the velocity dispersion (σ_v) of <40 km s^{-1} which results in an estimate of $V_{\rm rot}/\sigma > 2.5$. This result, if confirmed with higher resolution observations, would imply that kinematically cold discs are already in place at $z \sim 14$. Comparison with mock observations from the SERRA cosmological simulations confirms that even low-resolution observations are capable of detecting a velocity gradient in $z > 10$ galaxies as compact as JADES-GS-z14-0. This Letter shows that deeper ALMA or *JWST* (*James Webb Space Telescope*)/Near-Infrared Spectrograph integral field spectroscopy observations with high spatial resolution will be able to estimate an accurate dynamical mass for JADES-GS-z14-0, providing an upper limit to the stellar mass of this overluminous galaxy.

Key words: galaxies: evolution – galaxies: kinematics and dynamics.

1 INTRODUCTION

With the launch of the *James Webb Space Telescope* (*JWST*), we are now able to observe the rest-frame optical and ultraviolet (UV) emission from galaxies and their interstellar medium (ISM) up to redshift ∼14 (A. J. Cameron et al. 2023; E. Curtis-Lake et al. 2023; Y. Harikane et al. 2023, 2025; Y. Isobe et al. 2023; R. L. Larson et al. 2023; B. E. Robertson et al. 2023; S. Tacchella et al. 2023, 2025; Abdurro'uf et al. 2024; S. Carniani et al. 2024; T. Y.-Y. Hsiao et al. 2024; R. L. Sanders et al. 2024; A. Vikaeus et al. 2024), revealing a large population of bright, metal-poor galaxies in the early Universe. Remarkably, insight into the characteristics of the most distant galaxies can also be gained through interferometric observations, as illustrated by the detection of line emission from what is currently the most distant galaxy known [the Atacama Large Millimeter/submillimeter Array (ALMA); S. Carniani et al. 2025; S. Schouws et al. 2025b].

Before the launch of *JWST*, the main avenue to study the properties of high-redshift galaxies was with *Hubble Space Telescope* and ground-based 8–10 m observatories to study the rest-frame UV properties. Millimetre/submillimetre observatories such as ALMA and NOEMA (Northern Extended Millimeter Array) investigated these high-z galaxies through [C II] λ158 μm and [O III] λ88 μm emission lines and, in a few cases, far-infrared (FIR) continuum

★ E-mail: js2685@cam.ac.uk (JS); eleonora.parlanti@sns.it (EP)
† These authors contributed to this Letter equally.

emission. These observations revealed not only large dust reservoirs by $z \sim 8$ (Y. Tamura et al. 2019; T. J. L. C. Bakx et al. 2021; H. Inami et al. 2022; L. Sommovigo et al. 2022; J. Witstok et al. 2022), but also ISM properties such as metallicity and ionisztion parameter (J. S. Spilker et al. 2022; J. Witstok et al. 2022; M. Killi et al. 2023; K. C. Litke et al. 2023).

FIR observations of high-z galaxies also showed early rotating discs (e.g. R. Smit et al. 2018; M. Neeleman et al. 2020; F. Rizzo et al. 2020, 2021; F. Fraternali et al. 2021; F. Lelli et al. 2021; E. Parlanti et al. 2023; L. E. Rowland et al. 2024). However, in some cases, *JWST* observations have resolved these apparent discs into close-separation major mergers (e.g. F. Fraternali et al. 2021; I. Lamperti et al. 2024; H. Übler et al. 2024; G. C. Jones et al. 2025; E. Parlanti et al. 2025; J. Scholtz et al. 2025), although there is still debate over different kinematic signatures in cold and ionized gas phases. Theoretical models predict that high-redshift galaxies should be more turbulent, due to the increased merger rates (K. Duncan et al. 2019; Q. Duan et al. 2025), violent disc instabilities driven by the accretion of gas (A. Dekel et al. 2009; M. R. Krumholz et al. 2018), and intense star formation feedback (M. E. Orr et al. 2020). However, different cosmological simulations find different results, with some showing the presence of turbulent discs (A. Pillepich et al. 2019), while others predict that early galaxies should already have formed a cold rotating disc (M. Kohandel et al. 2024). This still leaves major questions about the assembly of discs at the epoch of reionization and beyond, including which gas phase best traces the galaxy kinematics/rotation.

The most distant spectroscopically confirmed galaxy is JADES-GS-53.08294-27.85563 (more commonly known as JADES-GS-z14-0; B. Robertson et al. 2024) at $z = 14.1796$, originally identified via Near-Infrared Camera (NIRCam) photometry (K. N. Hainline et al. 2024; B. Robertson et al. 2024) and later spectroscopically confirmed by Near-Infrared Spectrograph (NIRSpec; S. Carniani et al. 2024) and ALMA (S. Carniani et al. 2025; S. Schouws et al. 2025b). The combination of ALMA and *JWST* observations revealed a compact galaxy with a half-light radius of 260 ± 20 pc with metallicity of 0.1–0.2 $Z_\odot$, i.e. a significantly enriched ISM for $z \sim 14$ galaxy (S. Carniani et al. 2024). The galaxy is also detected at 7.7 μm with MIRI (Mid-Infrared Instrument) with strong excess to NIRCam photometry, indicating the presence of [O III] λλ5007, 4959 (J. M. Helton et al. 2025). Furthermore, S. Carniani et al. (2025) and S. Schouws et al. (2025b) detected [O III] λ88 μm in this galaxy with ALMA, measuring the dynamical mass from the velocity dispersion of the [O III] λ88 μm ($\log_{10}(M_{\rm dyn}/{\rm M}_\odot) = 9.0 \pm 0.2$), comparable to the galaxy's stellar mass ($\log_{10}(M_*/{\rm M}_\odot) = 8.7^{+0.7}_{-0.2}$). Under standard assumptions about stellar population modelling (e.g. G. Chabrier 2003 initial mass function; S. Carniani et al. 2025; J. M. Helton et al. 2025), the measured dynamical mass leaves very little mass budget for both gas and stars – the estimated gas fraction is only 10–30 per cent, making this galaxy gas-poor. This would be a result of either rapid gas consumption through previous star formation episodes or fast gas outflows ejecting the gas reservoir (S. Tacchella et al. 2016; A. Dekel et al. 2023; A. Ferrara 2024; A. Ferrara et al. 2025).

However, the dynamical mass estimates using the velocity dispersion of a line are notoriously uncertain, hence an accurate measurement of the dynamical mass with dynamical modelling is needed (M. Kohandel et al. 2019). In this Letter, we investigate the evidence for a velocity gradient using the ALMA observations of [O III] λ88 μm, to improve the measurement of the dynamical mass of JADES-GS-z14-0 and investigate the assembly of rotating discs in the early Universe.

Throughout this Letter, we adopt a flat ΛCDM (Λ cold dark matter) cosmology: $H_0 = 67.4$ km s^{-1} Mpc^{-1}, $\Omega_{\rm m} = 0.315$, and $\Omega_\Lambda = 0.685$ (Planck Collaboration VI 2020). With this cosmology, 1 arcsec corresponds to 3.3 kpc at $z = 14.18$.

2 OBSERVATIONS AND DATA REDUCTION

In this Letter, we use ALMA Band 6 observations of JADES-GS-z14-0 as part of 2023.A.00037.S programme (PI: Schouws), which used two spectral configurations to target the [O III] λ88 μm emission line. The total on-source integration time is 2.82 h per spectral configuration. We used the calibrated visibilities downloaded from the ALMA archive, only selecting the spectral configuration covering the detected [O III] λ88 μm emission line at 223.524 GHz, same data reduction as in S. Carniani et al. (2025).

In order to image the calibrated visibilities, we used the Common Astronomy Software Applications (CASA) package (J. P. McMullin et al. 2007; CASA Team 2022), specifically the task `tclean`. S. Carniani et al. (2025) and S. Schouws et al. (2025b) detected the emission line with 6.7σ. To optimize the spatial resolution of our observations while maintaining sufficient signal-to-noise ratio (S/N), we adopted Briggs weighting with a robust parameter of 0.5 and Hogbom deconvolver. We opted for a pixel scale of 0.1 arcsec, and a channel width of 10 km s^{-1} to create the final data cubes. We cleaned the images down to a 3σ level (rms = 0.1 mJy beam^{-1}). The final data cube has a resolution with a beam of 0.6 arcsec × 0.8 arcsec, compared to the deconvolved rest-frame UV half-light radius from NIRCam imaging of 0.079 arcsec and the natural weighting resolution of 1.09 arcsec × 0.82 arcsec used in S. Carniani et al. (2025) and S. Schouws et al. (2025b).

3 DETECTION AND MODELLING OF VELOCITY GRADIENT

3.1 Velocity gradient in [O III] λ88 μm

To investigate the presence of any velocity gradient traced by the [O III] λ88 μm emission line, we fitted each pixel of the data cube within a radius of <0.5 arcsec with a single Gaussian model, with centroid, velocity width, and amplitude as free parameters. We fitted this model using PYTHON's LMFIT. To construct the final map, we opted for an S/N cut-off of 3. We show the final velocity and full width at half-maximum (FWHM) maps of [O III] λ88 μm in the top and middle left panels of Fig. 1. The velocity map shows a velocity gradient in the north-east direction with velocities from +40 to −20 km s^{-1}. We verified this velocity gradient using three separate methods: (1) extracting integrated spectra from a grid of apertures; (2) performing spectro-astrometry in the image plane; and (3) performing spectro-astrometry in the *uv*-plane.

To confirm the velocity gradient, we extracted the regional spectra from a 3 × 3 square grid centred on the JADES-GS-z14-0. Each region has a size of 0.3 arcsec × 0.3 arcsec and we show these spectra on the right side of Fig. 1. We fitted the extracted spectra using a single Gaussian profile to determine the velocity centroid of the emission line profile. The extracted spectra confirm the presence of the velocity gradient in JADES-GS-z14-0 along the north-east direction with maximum velocity difference between two regions of 42 ± 14 km s^{-1}, which is significant at 3.0σ.

We further confirmed this velocity gradient using spectro-astrometry in both image and *uv*-plane. For the image plane analysis, we created two moment-0 maps of the [O III] λ88 μm emission line in the range [0, 50] km s^{-1} and [−50, 0] km s^{-1} to map the redshifted and

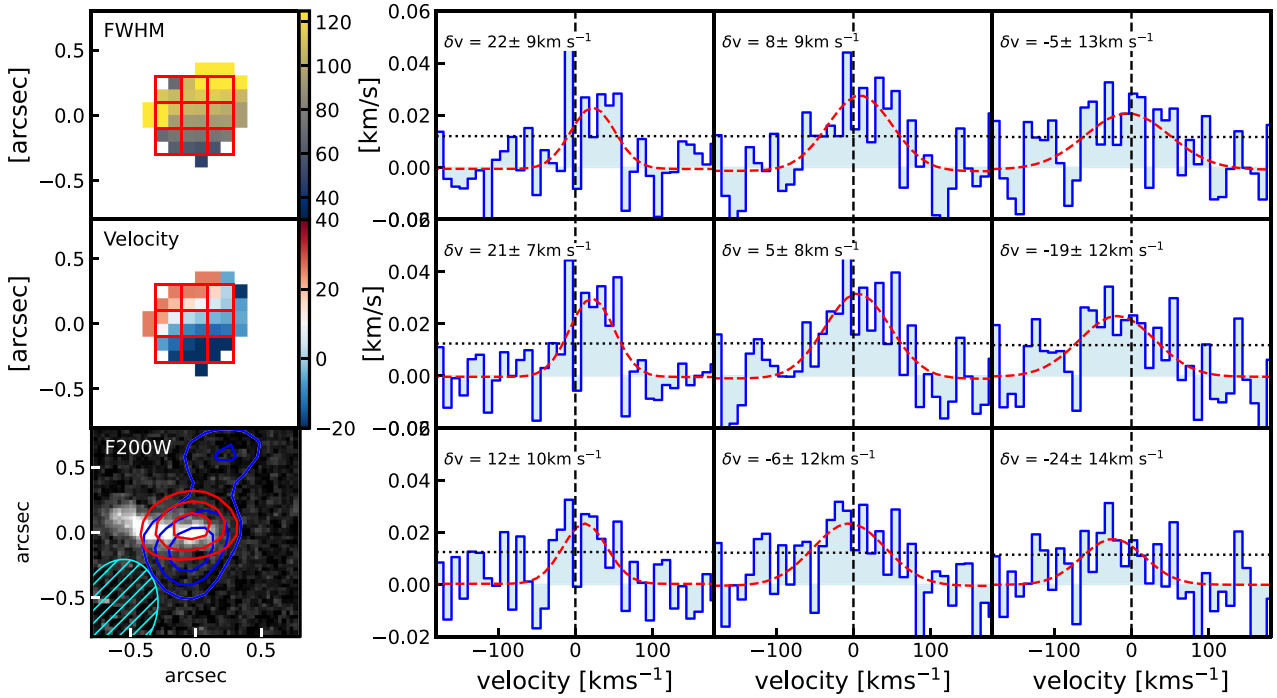

Figure 1. Tentative detection of the velocity gradient in JADES-GS-z14-0. Left top and middle panels: FWHM and velocity maps of the [O III] λ88 μm emission line from Gaussian fitting. We used a 3σ cut-off to create these maps. The red squares indicate the apertures used to extract spectra on the right. Bottom left: NIRCam *F200W* image tracing the rest-frame UV emission. The red and blue contours show moment-0 maps extracted from [−50, 0] km s^{-1} and [0, 50] km s^{-1}. The cyan-hatched ellipse shows the ALMA beam size. We observe 0.3 ± 0.06 arcsec ôffset between the red and blue centroids. Right panels: [O III] λ88 μm extracted from the square apertures indicated on velocity and FWHM maps. The data and the best-fitting model are shown as blue and red lines, while the black dotted line indicates the flux uncertainties. The extracted spectra confirm the derived velocity maps.

blueshifted parts of the emission line, respectively. These are shown as red and blue contours, respectively, on the moment-0 map in the bottom left panel of Fig. 1. We measure the spatial offset between the red and blue centroids of 0.30 ± 0.06 arcsec, corresponding to 0.99 ± 0.20 kpc.

We adopted a spectro-astrometry test in the *uv*-plane by performing a 2D Gaussian fitting to the *uv*-visibilities. We first extracted the *uv*-visibilities from the measurement set using spectral channels 66–70 for the blue side and channels 70–74 for the red side of the emission line, which corresponds to the [0, 50] km s^{-1} and [−50, 0] km s^{-1} channel maps. We fitted the model using an MCMC fitting routine (EMCEE; D. Foreman-Mackey et al. 2013), and we plot the final posterior distribution of the offsets between the location of the red and blue sides of the emission line and the centre of the galaxy in Fig. 2. The final estimated distance between the red and blue sides is 0.28 ± 0.10 arcsec (0.92 ± 0.33 kpc), clearly confirming the velocity gradient observed in the image plane. Furthermore, we split the observations into two exposures (1.4 h on source per exposure) and confirmed our findings in both exposures. Overall, all three approaches show tentative evidence for a velocity gradient in JADES-GS-z14-0.

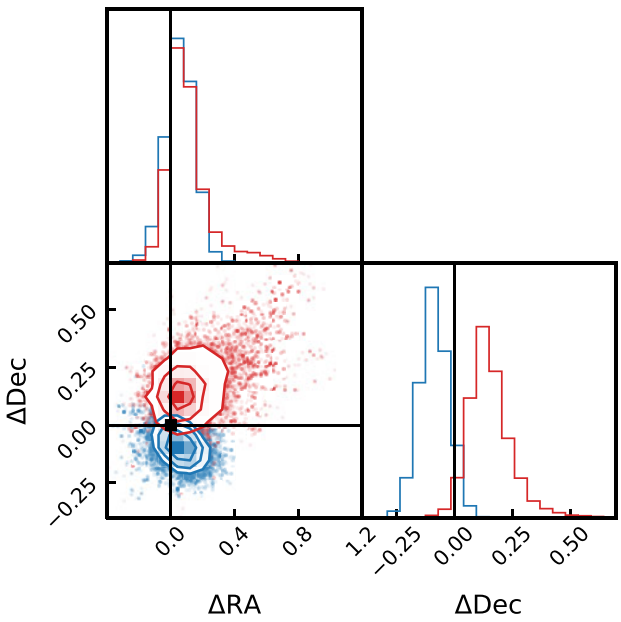

Figure 2. Spectro-astrometric analysis in the *uv*-plane. We show the posterior distribution of the spatial offset of the red and blue sides of the emission line from the centre of JADES-GS-z14-0 ([0, 50] km s^{-1} and [−50, 0] km s^{-1}). We see a spatial offset between the red and blue parts of the emission line, confirming the presence of the velocity gradient.

3.2 Modelling of the velocity gradient

In this section, we model the tentative velocity gradient detected in the previous section. Interpreting velocity gradients in low-resolution observations is challenging as mergers are often misinterpreted as rotating discs (e.g. M. Kohandel et al. 2020; F. Rizzo et al. 2022; E. Parlanti et al. 2025; J. Scholtz et al. 2025). However, in the NIRCam

images tracing the rest-frame UV (see Fig. 1), we do not see evidence of companions, double nuclei, tidal tails, or any other complex structure usually associated with merger events. The presence of an outflow causing the observed gradient is also excluded based on the low velocity dispersion of the observations. Within the S/N of our observations, we do not see clear traces of streams of inflowing gas that could lead to kinematic distortions and dynamical instabilities like those observed in other high-z systems (e.g. SPT 0311−58; S. Arribas et al. 2024). The measured offset of the red and blue centroids of [O III] λ88 μm spectrum is also well above the diffraction limit of *JWST* at 3 μm (0.1 arcsec), implying that any companion or tidal tails above this spatial scale would have been detected in the NIRCam images. Therefore, we will model this data by assuming it is a rotating disc.

We use the same method as described in E. Parlanti et al. (2023), using the publicly available PYTHON library KINMS (T. A. Davis, N. Zabel & J. M. Dawson 2020). Here, we briefly describe the procedure. This method creates a mock data cube of a rotating disc based on the input parameters, convolves it to match the spatial resolution of the observation to account for the beam-smearing effect, and then creates the model moment maps that we can directly compare with a set of observed ones. We set up KINMS to simulate the ALMA observations, with a spectral resolution of 10 km s^{-1}, and angular resolution set to the beam size of our observations (0.6 arcsec × 0.8 arcsec with an angle of 89°). To model the galaxy, we assume that the matter is distributed in a thin exponential disc (K. C. Freeman 1970) with an intrinsic constant velocity dispersion profile. We set a uniform prior on the σ_v between 0 and 200 km s^{-1}. Using this set-up, we generate a mock cube and moment maps which are compared to the observed ones. The best-fitting parameters are estimated using the package EMCEE (D. Foreman-Mackey et al. 2013). We used uniform priors on the inclination between 5° and 85°, and uniform priors on the position angle between 0° and 180°. The dynamical mass was left free to vary with log uniform priors between 10^8 and 10^{11} M$_\odot$, and we assumed uniform priors on the velocity dispersion between 5 and 200 km s^{-1}. We masked the pixels in the moment-2 map with FWHM > 150 km s^{-1} as they are dominated by noise in the outskirts of the galaxy.

We fitted simultaneously the velocity and velocity dispersion maps derived in Section 3.1 to estimate the inclination of the disc, dynamical mass, position angle, and intrinsic velocity dispersion (i.e. deconvolved by the instrumental spatial resolution), while we fixed the disc effective radius to the one found in S. Carniani et al. (2024) from NIRCam imaging of 260 pc (0.079 arcsec). We note that the stellar and ionized gas sizes were found to be comparable in the Integral Field Unit (IFU) observations (e.g. J. Scholtz et al. 2018; N. M. Förster Schreiber et al. 2019).

We show the comparison of the data and the fitted model in Fig. 3. We note that the model is not fully able to reproduce the observed velocity gradient, due to the low value of the observed velocity dispersion. To reproduce the observed velocity gradient, the beam-smearing effect does increase the observed velocity dispersion. Modelling only the velocity gradient would improve the fit of the velocity map and result in a higher dynamical mass, but would overestimate the observed velocity dispersion map. In this Letter, we used the approach of fitting the maps simultaneously. With low-resolution data, the beam-smearing effect causes the observed velocity dispersion to be affected by the underlying velocity gradient, adding little constraint to the overall fit. Higher resolution observations would decrease the level of beam smearing, allowing for more accurate modelling.

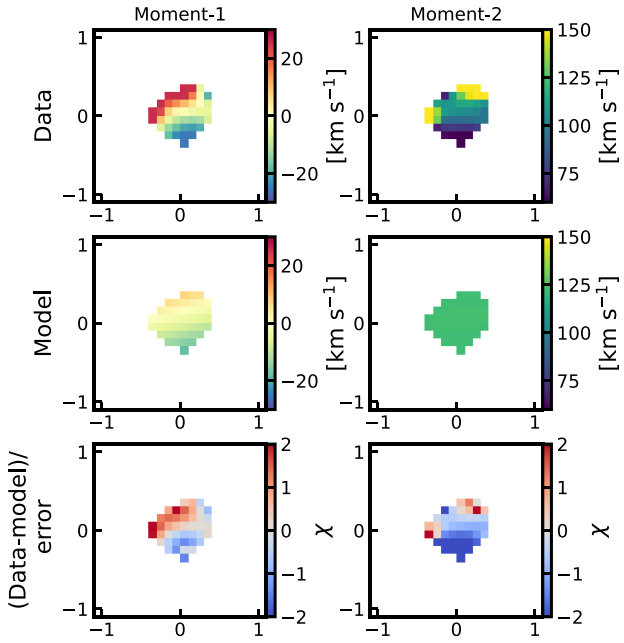

Figure 3. Moment maps created from the observed data (top row), maps from the best-fitting kinematical model of KINMS (centre row), and the normalized residuals (bottom row). The left and right columns show moment-1 and moment-2 maps, respectively.

Due to the low resolution of the data, we cannot simultaneously obtain tight constraints on the inclination and the dynamical mass of the system as they are degenerate (in low-resolution observations, models with constant $M_{\rm dyn}\sin^2$(inc) are similar, see Fig. A1). Due to the form of the degeneracy, even when the inclination is unconstrained, we are able to estimate, with large uncertainties, the dynamical mass of the system, obtaining a value of $\log(M_{\rm dyn}/{\rm M}_\odot) = 9.4^{+0.8}_{-0.4}$. Assuming that the mass is distributed as an exponential disc with the fixed effective radius of 260 pc and the dynamical mass obtained by the kinematic modelling, we computed the rotational velocity as the maximum velocity of the rotating disc occurring at $2.2r_{\rm d} \sim 340$ pc. With these assumptions, we obtain an estimate of the rotational velocity of $V_{\rm rot} = 164^{+248}_{-60}$ km s^{-1}. Interestingly, we find a 3σ upper limit on the intrinsic velocity dispersion of <40 km s^{-1} (3σ upper limit). This would result in an estimation of $V_{\rm rot}/\sigma_v > 2.5$, which would imply tentative evidence for a kinematically cold disc in the first 300 Myr of the Universe's lifetime. We compare our measurement of $V_{\rm rot}/\sigma_v$ with simulations and observations compiled from the literature by placing this estimate on a plot of $V_{\rm rot}/\sigma_v$ versus redshift (see Fig. 4). We find that our measured tentative value for JADES-GS-z14-0 aligns with simulation predictions. It follows the evolutionary trend of $M_* > 10^9$ M$_\odot$ systems at $z > 6$. If confirmed, this would be the most distant dynamically settled disc structure observed to date.

Our measurement of $M_{\rm dyn}$ is consistent within 1σ with the values measured by S. Carniani et al. (2025) ($\log(M_{\rm dyn}/{\rm M}_\odot) = 9.0 \pm 0.2$) and by S. Schouws et al. (2025b) ($\log(M_{\rm dyn}/{\rm M}_\odot) = 9.0 \pm 0.3\sin(i)^2$) from the velocity dispersion of the [O III] λ88 μm, but our error bars fully capture the additional uncertainty due to the mass–inclination degeneracy. We derive a gas fraction of this galaxy of 60 ± 20 per cent, consistent with the value derived by previous analysis of the [O III] λ88 μm observations of 36 per cent (S.

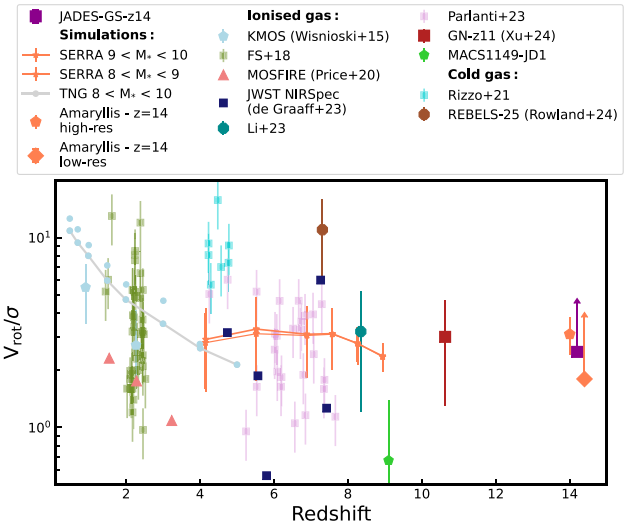

Figure 4. $V_{\rm rot}/\sigma_v$ versus redshift for observations and simulations. As we are unable to constrain the velocity dispersion of JADES-GS-z14-0 and in the low-resolution mock observations of 'Amaryllis' from SERRA simulations, we only quote a lower limit on $V_{\rm rot}/\sigma_v$ for these. We compare JADES-GS-z14-0 to a compilation from the literature: *JWST*/NIRSpec, IllustrisTNG (A. Pillepich et al. 2019), SERRA (M. Kohandel et al. 2024), ground-based IFU (E. Wisnioski et al. 2015; N. M. Förster Schreiber et al. 2018), MOSFIRE (S. H. Price et al. 2020), GN-z11 (Y. Xu et al. 2024), ALMA $z \sim 6$ (E. Parlanti et al. 2023), NIRSpec/MSA (A. Graaff et al. 2024), ALMA $z \sim 4$ (F. Rizzo et al. 2021), REBELS-25 (L. E. Rowland et al. 2024), MACS 1149-JD1 (T. Tokuoka et al. 2022), and MACS 0416-Y3 (Z. Li et al. 2023).

Carniani et al. 2025; S. Schouws et al. 2025b) and <70 per cent (S. Schouws et al. 2025a). However, for better constraints on the kinematics of JADES-GS-z14-0, we require higher sensitivity and resolution observations from ALMA or *JWST*/NIRSpec-integral field spectroscopy (IFS; see the results of our simulations in Section 4).

We also fitted the 1D velocity and velocity dispersion profiles, and the moment maps by using the dynamical fitting code DYSMALPY (S. H. Price et al. 2021; L. L. Lee et al. 2025), which has proven to be a reliable method to recover the kinematical properties of data sets with low S/N and low spatial resolution. With this method, we obtain comparable results (within 1σ) for the dynamical mass and the velocity dispersion.

4 COMPARISON TO SERRA SIMULATIONS

We compare our results against mock [O III] λ88 µm data generated from the SERRA suite of zoom-in, high-resolution cosmological simulations (A. Pallottini et al. 2022). These simulations achieve a mass resolution of 1.2×10^4 M$_\odot$, ~25 pc at $z = 7.7$, and incorporate non-equilibrium chemistry with on-the-fly radiative transfer. Their outputs are subsequently post-processed to generate FIR emission lines (A. Pallottini et al. 2019) and hyperspectral data cubes (M. Kohandel et al. 2020), well-suited for producing realistic mock observations of the early Universe. In particular, we use the simulated galaxy 'Amaryllis', identified by M. Kohandel et al. (2023) as the brightest galaxy ($\log(L_{\rm [O\,III]\,88\,\mu m}/{\rm L}_\odot) \approx 8.4$) in SERRA at $11 < z < 14$. Amaryllis has a stellar mass $\log(M_\star/{\rm M}_\odot) \approx 8.8$ and ${\rm SFR}_{10\,{\rm Myr}} = 18\,{\rm M}_\odot\,{\rm yr}^{-1}$, making it a close analogue to JADES-GS-z14-0. To generate synthetic ALMA observations, we select a viewing angle of 45°, at which the FWHM of the [O III] λ88 µm emission line closely matched that of JADES-GS-z14-0. The effective radius of Amaryllis is ~180 pc, while JADES-GS-z14-0 has a size of 260 pc. To match this scale, we rescale the mock data by a factor of 1.5 to improve the comparison between the mock observations and JADES-GS-z14-0.

We used CASA's `simobserve` with an array configuration of C5 and C7 corresponding to a resolution of 0.8 and 0.15 arcsec, respectively. We use integration times of 2.85 and 10.0 h for the C5 and C7 array configurations, respectively, to match the S/N of our current observations and of potential future deeper, higher resolution ALMA and NIRSpec/IFS observations. We show the moment maps of Amaryllis (flux, velocity, and FWHM) in Fig. 5 for the low- and high-resolution observations.

The mock observations from the SERRA simulations in Fig. 5 show that a velocity gradient in a rotating galaxy at $z > 10$ like JADES-GS-z14-0 can be detected even in low-resolution observations (see top row of Fig. 5). We modelled the mock observations using the same modelling set-up described in Section 3.2. Despite detecting the velocity gradient in the low-resolution mock observations of Amaryllis simulations, we encountered similar degeneracies between inclination and dynamical mass as for the ALMA observations of JADES-GS-z14-0, and we can only estimate an upper limit to the velocity dispersion, therefore, we are only able to estimate a lower limit on $V_{\rm rot}/\sigma_v > 1.8$. However, using high spatial resolution observations (~0.15 arcsec), which are achievable by both *JWST*/NIRSpec and ALMA observations, it would be possible to resolve these high-z targets with more than three independent resolution elements (see beam size in Fig. 5), which is the required condition to properly constrain a galaxy kinematics and distinguish rotating discs from close mergers (F. Rizzo et al. 2022). Indeed, we tested a merger scenario of Amaryllis from the SERRA simulations in Appendix B, showing that we are capable of distinguishing between a merger and disc rotation scenario with high-resolution observations. For *JWST*/NIRSpec-IFS observation, we would need to target the C III] $\lambda\lambda$1907, 1909 emission line doublet as it is the only detected emission line in the current spectrum, requiring the on-source exposure time of over ~50 h. However, given the point spread function size of 0.15 arcsec, these observations would be able to resolve the blue and red sides of the emission, as measured in Section 3.1. With such deeper high-resolution observations, it would be possible to break the degeneracy between the dynamical mass and inclination (see Fig. A1, right panel) with a measured value of $V_{\rm rot}/\sigma_v = 3.1 \pm 0.7$ and an uncertainty on the dynamical mass of 0.2 dex. This clearly shows that a follow-up with deep *JWST*/NIRSpec-IFS or ALMA observations is essential to constrain the kinematics of JADES-GS-z14-0.

5 CONCLUSIONS

In this Letter, we re-examined the ALMA observations of [O III] λ88 µm emission line in JADES-GS-z14-0 at $z \sim 14.2$, to constrain its kinematic properties. We created velocity maps by fitting a Gaussian profile to [O III] λ88 µm emission line, and we found evidence for a velocity gradient in the data with a maximum velocity difference of 50 km s^{-1} in the north–south direction. We confirmed the presence of the velocity gradient by (1) extracting regional spectra from nine regions (see Fig. 1) and (2) performing spectro-astrometry in the image and *uv* planes, which found a spatial offset of 0.28 ± 0.10 arcsec between the redshifted and blueshifted parts of the emission line (see Figs 1 and 2). Using these approaches, we found similar velocity gradients.

Due to the lack of merger signatures and/or streams of gas associated with outflows and accretion of gas in the NIRCam imaging, we

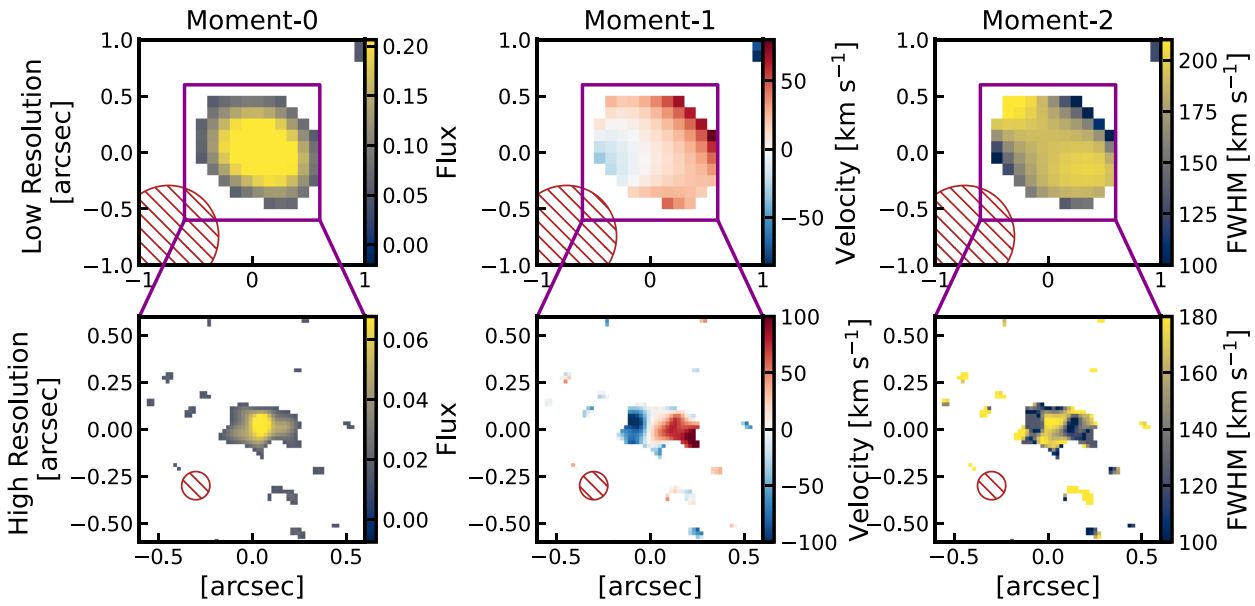

Figure 5. Mock observations of JADES-GS-z14-0 analogue in the SERRA simulations – 'Amaryllis'. The top row shows flux, velocity, and FWHM maps of mock low-resolution ALMA observations (0.9 arcsec), while the bottom row shows mock high-resolution observations (0.15 arcsec). The simulations show that a rotating galaxy shows a small velocity gradient (<40 km s^{-1}) in the low-resolution data, similar to our observations. The simulations show that a rotating (thin) disc galaxy with a size and mass as JADES-GS-z14-0, and observed under similar conditions, should show a similar velocity gradient to the one obtained. The increased FWHM in the centre of high-resolution observations can be due to the beam smearing of the rotation.

modelled the galaxy kinematics assuming a thin rotating disc of size 260 pc. We measured a dynamical mass of $\log(M_{\rm dyn}/{\rm M}_\odot) = 9.4^{+0.8}_{-0.4}$. Our large uncertainties reflect the inability of the data with low spatial resolution to break the degeneracy between dynamical mass and inclination. However, our model fully captures this additional uncertainty, which is not accounted for by the virial estimator. We estimated a lower limit on the $V_{\rm rot}/\sigma_v$ of >2.5, which would indicate a dynamically settled cold at these high redshifts if confirmed.

We compared our observational results with mock observations from the SERRA cosmological simulations. We created mock ALMA [O III] λ88 μm observations of an analogue of JADES-GS-z14-0 called 'Amaryllis', with both low and high spatial resolution set-ups (0.8 and 0.15 arcsec). We show that the tentative detection of the velocity gradient is possible even in the low-resolution data (see the top row of Fig. 5). However, in order to break the degeneracy between dynamical mass and inclination, high spatial resolution observations (<0.2 arcsec) are required. These high spatial resolution observations could confirm the high $V_{\rm rot}/\sigma_v$ in the galaxy and constrain the dynamical mass within 0.23 dex.

Our tentative detection of this velocity gradient suggests that the formation of early cold rotating structures in the Universe happened much sooner than previously anticipated in both observations and simulations. The discovery of a rotation-dominated disc just 300 Myr after the big bang would drastically change our view of early galaxies, and pose new challenges to the cosmological simulations, while putting constraints on feedback models. However, due to the limited resolution of the current observation, we can only obtain a tentative detection of the presence of an early rotating disc. Further high spectral and higher spatial resolution deep observations with ALMA and *JWST* IFU are essential in order to resolve the kinematics of JADES-GS-z14-0 and investigate the formation of discs in the early Universe.

ACKNOWLEDGEMENTS

This Letter makes use of the following ALMA data: ADS/JAO.ALMA#2023.A.00037.S. ALMA is a partnership of ESO (representing its member states), NSF (USA), and NINS (Japan), together with NRC (Canada), MOST and ASIAA (Taiwan), and KASI (Republic of Korea), in cooperation with the Republic of Chile. The Joint ALMA Observatory is operated by ESO, AUI/NRAO, and NAOJ. The National Radio Astronomy Observatory is a facility of the National Science Foundation operated under a cooperative agreement by Associated Universities, Inc. JS, FDE, RM, and GCJ acknowledge support by the Science and Technology Facilities Council (STFC), ERC Advanced Grant 695671 'QUENCH', and the UKRI Frontier Research grant RISEandFALL. RM also acknowledges funding from a research professorship from the Royal Society. SC, EP, and GV acknowledge support from the European Union (ERC, WINGS, 101040227). ALD thanks the University of Cambridge Harding Distinguished Postgraduate Scholars Programme and Science and Technology Facilities Council (STFC) Centre for Doctoral Training (CDT) in Data Intensive Science at the University of Cambridge (STFC grant number 2742605) for a PhD studentship. SA acknowledges grant PID2021-127718NB-I00 funded by the Spanish Ministry of Science and Innovation/State Agency of Research (MICIN/AEI/ 10.13039/501100011033) AJB acknowledges funding from the 'FirstGalaxies' Advanced Grant from the European Research Council (ERC) under the European Union's Horizon 2020 Framework Programme (grant agreement no. 789056). ZJ acknowledges *JWST*/NIRCam contract to the University of Arizona, NAS5-02015. BR acknowledges support from the NIRCam Science Team contract to the University of Arizona, NAS5-02015, and *JWST* Program 3215. We acknowledge the CINECA award under the ISCRA initiative, for the availability of high-performance computing resources and support from the Class B project SERRA HP10BPUZ8F (PI: Pallottini). We gratefully acknowledge the com-

putational resources of the Center for High Performance Computing (CHPC) at SNS. HÜ acknowledges support through the ERC Starting Grant 101164796 'APEX'. IS acknowledges support from PID2022-140483NB-C22 funded by AEI 10.13039/501100011033 and BDC 20221289 funded by MCIN by the Recovery, Transformation and Resilience Plan from the Spanish State, and by NextGenerationEU from the European Union through the Recovery and Resilience Facility. SA acknowledges grant PID2021-127718NB-I00 funded by the Spanish Ministry of Science and Innovation/State Agency of Research (MICIN/AEI/10.13039/501100011033).

DATA AVAILABILITY

The data sets were derived from sources in the public domain: ALMA data from https://almascience.nrao.edu/aq/?result_view=observation.

REFERENCES

Abdurro'uf et al., 2024, ApJ, 973, 47
Arribas S. et al., 2024, A&A, 688, A146
Bakx T. J. L. C. et al., 2021, MNRAS, 508, L58
Cameron A. J. et al., 2023, A&A, 677, A115
Carniani S. et al., 2024, Nature, 633, 318
Carniani S. et al., 2025, A&A, 696, A87
CASA Team, 2022, PASP, 134, 114501
Chabrier G., 2003, PASP, 115, 763
Curtis-Lake E. et al., 2023, Nat. Astron., 7, 622
Davis T. A., Zabel N., Dawson J. M., 2020, Astrophysics Source Code Library, record ascl:2006.003
de Graaff A. et al., 2024, A&A, 684, A87
Dekel A. et al., 2009, Nature, 457, 451
Dekel A., Sarkar K. C., Birnboim Y., Mandelker N., Li Z., 2023, MNRAS, 523, 3201
Duan Q. et al., 2025, MNRAS, 540, 774
Duncan K. et al., 2019, ApJ, 876, 110
Ferrara A., 2024, A&A, 689, A310
Ferrara A., Carniani S., di Mascia F., Bouwens R. J., Oesch P., Schouws S., 2025, A&A, 694, A215
Foreman-Mackey D., Hogg D. W., Lang D., Goodman J., 2013, PASP, 125, 306
Förster Schreiber N. M. et al., 2018, ApJS, 238, 21
Förster Schreiber N. M. et al., 2019, ApJ, 875, 21
Fraternali F., Karim A., Magnelli B., Gómez-Guijarro C., Jiménez-Andrade E. F., Posses A. C., 2021, A&A, 647, A194
Freeman K. C., 1970, ApJ, 160, 811
Hainline K. N. et al., 2024, ApJ, 976, 160
Harikane Y. et al., 2023, ApJS, 265, 5
Harikane Y. et al., 2025, ApJ, 980, 138
Helton J. M. et al., 2025, Nat. Astron., 9, 729
Hsiao T. Y.-Y. et al., 2024, ApJ, 973, 8
Inami H. et al., 2022, MNRAS, 515, 3126
Isobe Y. et al., 2023, ApJ, 959, 100
Jones G. C. et al., 2025, MNRAS, 540, 3311
Killi M. et al., 2023, MNRAS, 521, 2526
Kohandel M., Pallottini A., Ferrara A., Zanella A., Behrens C., Carniani S., Gallerani S., Vallini L., 2019, MNRAS, 487, 3007
Kohandel M., Pallottini A., Ferrara A., Carniani S., Gallerani S., Vallini L., Zanella A., Behrens C., 2020, MNRAS, 499, 1250
Kohandel M., Ferrara A., Pallottini A., Vallini L., Sommovigo L., Ziparo F., 2023, MNRAS, 520, L16
Kohandel M., Pallottini A., Ferrara A., Zanella A., Rizzo F., Carniani S., 2024, A&A, 685, A72
Krumholz M. R., Burkhart B., Forbes J. C., Crocker R. M., 2018, MNRAS, 477, 2716
Lamperti I. et al., 2024, A&A, 691, A153
Larson R. L. et al., 2023, ApJ, 953, L29
Lee L. L. et al., 2025, ApJ, 978, 14
Lelli F., Di Teodoro E. M., Fraternali F., Man A. W. S., Zhang Z.-Y., De Breuck C., Davis T. A., Maiolino R., 2021, Science, 371, 713
Li Z. et al., 2023, preprint (arXiv:2310.09327)
Litke K. C. et al., 2023, ApJ, 949, 87
McMullin J. P., Waters B., Schiebel D., Young W., Golap K., 2007, in Shaw R. A., Hill F., Bell D. J., eds, ASP Conf. Ser. Vol. 376, Astronomical Data Analysis Software and Systems XVI. Astron. Soc. Pac., San Francisco, p. 127
Neeleman M., Prochaska J. X., Kanekar N., Rafelski M., 2020, Nature, 581, 269
Orr M. E. et al., 2020, MNRAS, 496, 1620
Pallottini A. et al., 2019, MNRAS, 487, 1689
Pallottini A. et al., 2022, MNRAS, 513, 5621
Parlanti E., Carniani S., Pallottini A., Cignoni M., Cresci G., Kohandel M., Mannucci F., Marconi A., 2023, A&A, 673, A153
Parlanti E. et al., 2025, A&A, 695, A6
Pillepich A. et al., 2019, MNRAS, 490, 3196
Planck Collaboration VI, 2020, A&A, 641, A6
Price S. H. et al., 2020, ApJ, 894, 91
Price S. H. et al., 2021, ApJ, 922, 143
Rizzo F., Vegetti S., Powell D., Fraternali F., McKean J. P., Stacey H. R., White S. D. M., 2020, Nature, 584, 201
Rizzo F., Vegetti S., Fraternali F., Stacey H. R., Powell D., 2021, MNRAS, 507, 3952
Rizzo F., Kohandel M., Pallottini A., Zanella A., Ferrara A., Vallini L., Toft S., 2022, A&A, 667, A5
Robertson B. E. et al., 2023, Nat. Astron., 7, 611
Robertson B. et al., 2024, ApJ, 970, 31
Rowland L. E. et al., 2024, MNRAS, 535, 2068
Sanders R. L., Shapley A. E., Topping M. W., Reddy N. A., Brammer G. B., 2024, ApJ, 962, 24
Scholtz J. et al., 2018, MNRAS, 475, 1288
Scholtz J. et al., 2025, MNRAS, 539, 2463
Schouws S. et al., 2025a, preprint (arXiv:2502.01610)
Schouws S. et al., 2025b, ApJ, 988, 19
Smit R. et al., 2018, Nature, 553, 178
Sommovigo L. et al., 2022, MNRAS, 513, 3122
Spilker J. S. et al., 2022, ApJ, 929, L3
Tacchella S., Dekel A., Carollo C. M., Ceverino D., DeGraf C., Lapiner S., Mandelker N., Primack Joel R., 2016, MNRAS, 457, 2790
Tacchella S. et al., 2023, MNRAS, 522, 6236
Tacchella S. et al., 2025, MNRAS, 540, 851
Tamura Y. et al., 2019, ApJ, 874, 27
Tokuoka T. et al., 2022, ApJ, 933, L19
Übler H. et al., 2024, MNRAS, 533, 4287
Vikaeus A. et al., 2024, MNRAS, 529, 1299
Wisnioski E. et al., 2015, ApJ, 799, 209
Witstok J. et al., 2022, MNRAS, 515, 1751
Xu Y. et al., 2024, ApJ, 976, 142

APPENDIX A: POSTERIOR DISTRIBUTION OF KINEMATICAL FITTING

We present the posterior distribution of our kinematical modelling of the ALMA data of JADES-GS-z14-0 and the mock observations of the galaxy Amaryllis from SERRA cosmological simulations (both low and high resolution) in Fig. A1.

APPENDIX B: ALMA MOCK OBSERVATION OF AMARYLLIS DURING A MERGER

In Fig. B1, we explore a snapshot of the SERRA simulations where Amaryllis is merging with a close by galaxy. In the low-resolution observations (top row), the observations would produce a similar

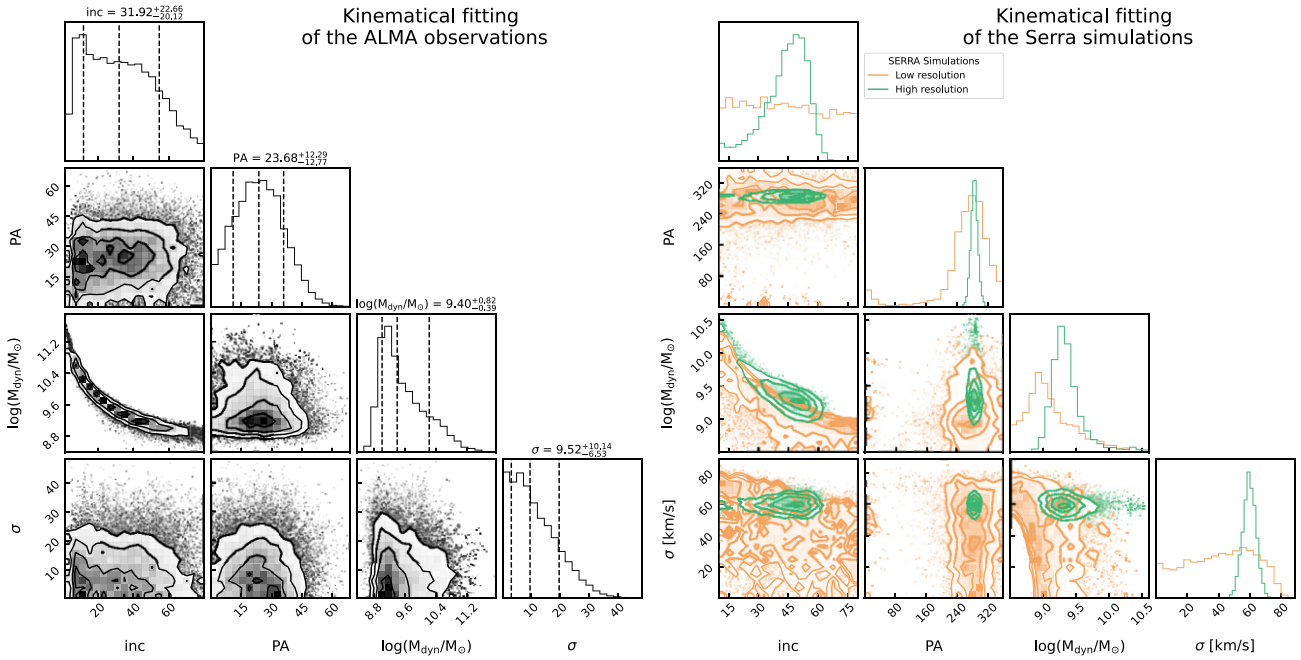

Figure A1. Posterior distribution from the kinematical modelling of ALMA data of JADES-GS-z14-0 (left panel) and mock observations of the galaxy Amaryllis from SERRA simulations (right panel).

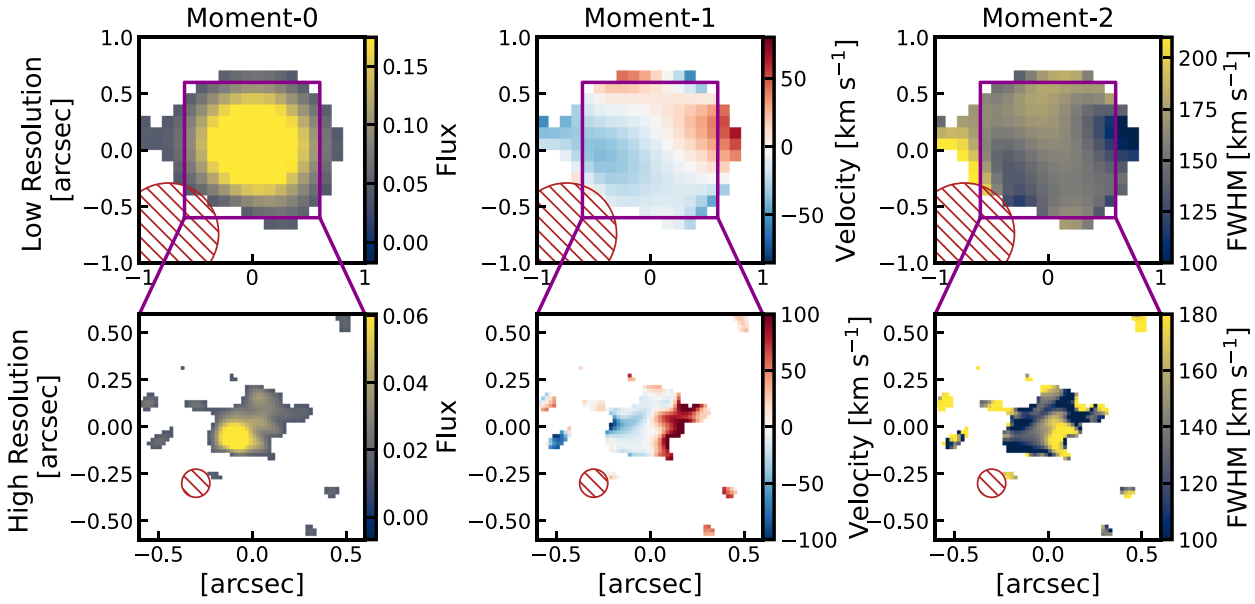

Figure B1. Mock observations of JADES-GS-z14-0 analogue in the SERRA simulations, 'Amaryllis', during a merger event. The top row shows flux, velocity, and FWHM maps of mock low-resolution ALMA observations (0.9 arcsec), while the bottom row shows mock high-resolution observations (0.15 arcsec). The simulations show that a rotating galaxy shows a small velocity gradient (<40 km s^{-1}) in the low-resolution data, similar to our observations. The simulations show that a rotating (thin) disc galaxy with a size and mass as JADES-GS-z14-0, and observed under similar conditions, should show a similar velocity gradient to the one obtained.

velocity gradient; however, such a companion would easily be seen in the NIRCam photometry. However, the high-resolution ALMA or *JWST* data could easily distinguish between a merger and rotating scenario, as there would be a clearly visible tail in the moment-0 map as well as a clearly disturbed velocity field and velocity dispersion map.

This paper has been typeset from a TEX/LATEX file prepared by the author.